



UPPSALA
UNIVERSITET

Independent Project at the Department of Earth Sciences
Självständigt arbete vid Institutionen för geovetenskaper
2017:22

Modelling the Formation and Propagation of Orographic Rossby Waves

Modellering av formation och propagering
av orografiska Rossbyvågor

Eskil Jonsson

Independent Project at the Department of Earth Sciences
Självständigt arbete vid Institutionen för geovetenskaper
2017:22

Modelling the Formation and Propagation of Orographic Rossby Waves

Modellering av formation och propagering
av orografiska Rossbyvågor

Eskil Jonsson

Sammanfattning

Modellering av formation och propagering av orografiska Rossbyvågor

Eskil Jonsson

Orografiska Rossby-vågor är den huvudsakliga mekanismen genom vilken jetströmmarna slingrar runt jorden och kan ha en omfattande inverkan på väder och klimat (kapitel 1). Därför är de av särskild betydelse att studera och detta projekt bör fungera som en utgångspunkt för vad man måste överväga när man försöker modellera dessa vågor. Till exempel så måste vi ta hänsyn till tryckgradienter, Coriolis-effekten, orografi, potentiell vorticetsbevarande och även jordens krökning på denna skala. Dessa beskrivs i detalj i kap. 2 och anpassas till rörelseekvationerna för grunt vatten (Saint-Venant-ekvationerna). Därefter presenteras några numeriska tekniker på grundläggande nivå för att lösa dessa ekvationer i kap. 2.4, varvid de sedan implementeras för de globala Saint-Venant-ekvationerna med bevarad potentiell vorticitet i kap 3. Modellen är validerad för typiska grunda vattenflöden i ett badkar och passerar vanliga numeriska tester så som Gauss-kurvtestet (kap. 4.1). Men när vi överväger atmosfäriska flöden (kap. 4.2) blir det tydligt att våra modeller och numeriska metoder är primitiva och inte kan reproducera Rossby-vågor på ett stabilt sätt. Därmed, modifierar vi Hogans modell (Hogan, n.d) för att passa vår modell vilket resulterar orografiska Rossby-vågor. Dock så är dessa förskjutna och stämmer inte riktigt överens med teorin i kap. 2.2. Även Hogans modell visar sig ha allvarliga begränsningar då vågorna propagerar i fel riktning. Därmed är denna studie ej komplett och kräver ytterligare utveckling för att vara användbar.

Nyckelord: Global modell, grund fluid approximation, mellan-övre troposfären, potentiell vorticetsbevarande

Examensarbete C i meteorologi, 1ME420, 15 hp, 2017

Handledare: Björn Claremar

Institutionen för geovetenskaper, Uppsala universitet, Villavägen 16, 752 36 Uppsala
(www.geo.uu.se)

Hela publikationen finns tillgänglig på www.diva-portal.org

Abstract

Modelling the Formation and Propagation of Orographic Rossby Waves

Eskil Jonsson

Orographic Rossby waves are the main mechanism by which the jet streams meander around the Earth and have possibly far-reaching impacts on weather and climate (chapter 1). Hence, they are of particular importance to study and this project should serve as a starting point in what to consider when trying to model these waves. For example, we have to account for pressure gradients, Coriolis effect, orography, potential vorticity conservation and also Earth's curvature at this scale. These are covered in detail in ch. 2 and adapted to the Shallow Water Equations. In addition, some entry-level numerical techniques for solving these equations are presented throughout ch. 2.4 and then implemented for the global-scale Shallow Water Equations with conserved potential vorticity in ch. 3. The model is validated to work for typical shallow water flows in a bath tub and passes common tests like the Gaussian curve test (ch. 4.1). However, when considering atmospheric flows (ch. 4.2) it becomes evident that our model, as well as our numerical methods are lacking and cannot reproduce Rossby waves in a stable manner. Hence, a heavily modified version of Hogan's model (Hogan, n.d) is employed with a simplified numerical scheme. With these corrections, orographic Rossby waves appear to naturally form at appropriate locations. However, they do not fully exhibit the expected behaviours discussed in ch. 2.2. Even Hogan's model appears to have severe limitations as waves propagate in the wrong direction. Hence, this study is not complete and warrants further development in order to be useful.

Keywords: Global model, shallow fluid approximation, middle-high troposphere, potential vorticity conservation

Degree Project C in Meteorology, 1ME420, 15 credits, 2017

Supervisor: Björn Claremar

*Department of Earth Sciences, Uppsala University, Villavägen 16, SE-752 36 Uppsala
(www.geo.uu.se)*

The whole document is available at www.diva-portal.org

Foreword

Before reading this paper the reader should have a basic understanding of meteorology and fluid dynamics. Numerical techniques of solving partial differential equations will be covered from the basics, though some previous exposure to scientific computing is recommended. Some caveats to keep in mind is that the results presented in this paper are very preliminary and subject to large errors. There was insufficient time to cover the modelling trials extensively since most of the focus of this project had to go towards implementing a working model that was stable. Although theoretically simple and feasible, in practicality it becomes much more difficult.

Contents

1	Introduction	1
2	Review	1
2.1	Jet Streams and their Impacts on Climate	1
2.2	Rossby Wave Formation and Propagation	3
2.2.1	The Vorticity Equation	3
2.2.2	Barotropic Potential Vorticity Conservation	5
2.3	The Global-Scale Shallow Water Equations	7
2.3.1	Shallow Water Continuity Equation	7
2.3.2	Curvature, and Potential Vorticity in the Shallow Water Momentum Equations	8
2.4	Numerical Techniques	10
2.4.1	The Forward-Time Central Space Scheme	11
2.4.2	Convergence, Consistency, and Stability	12
2.4.3	The Lax-Friedrichs Scheme	12
2.4.4	The Leapfrog Scheme	13
2.4.5	The Lax-Wendroff Scheme	13
2.4.6	Boundary Conditions	14
3	Methodology	15
3.1	Orography and β -Plane Approximation	15
3.2	Initial Conditions	17
3.3	Solving the System of Equations	18
4	Results and Discussion	18
4.1	Effects of Artificial Viscosity	19
4.2	Orographic Rossby Waves	19
5	Summary and Conclusions	23
6	Acknowledgements	24
7	Software	26
A	Appendices	27
A Additional Numerical Methods	27	
A.1	Dimensional Splitting	27
A.2	Artificial Viscosity	27
B	MATLAB Code	28
B.1	Spatial Domain and Parameters	28
B.2	Orography Pre-processing	28
B.3	Coriolis Parameter	28
B.4	Initial Conditions	29
B.4.1	Geostrophic Balance	29
B.5	While-Loop	29
B.6	Lax-Wendroff Scheme	29
B.7	Boundary Conditions	30
B.8	Dimensionally Split Lax-Friedrich Scheme	30
C	Additional Figures	32
C.1	Semi-Permanent Pressure Zones	32

1 Introduction

Due to accumulating evidence implicating the impact of Rossby waves on climate and weather, such as their role in Arctic warming, we sought to develop a simple numerical model of these waves that can be used to assess these impacts. This paper serves as a first introduction on this topic and reviews the basics of Rossby-wave formation and propagation, numerical models for solving the equations of motion governing them, and illustrating some of the pitfalls students may encounter while doing so. For example, what are the assumptions that can be made when dealing with Rossby waves and how do features such as orography, Coriolis, and Earth's curvature impact them? Additionally, how is the numerical model implemented and what are the criteria it has to meet? Questions such as these are addressed throughout the paper and some preliminary results of these implementations are showcased.

As a quick introduction; Rossby waves are synoptic- to planetary-scale atmospheric or oceanic waves that arise from the fluid-dynamical analogue of conservation of angular momentum—namely conservation of potential vorticity. This quantity is determined by latitude and the elevation profile of the underlying topography (or orography). Hence, Rossby waves are sometimes termed mountain waves as they tend to form around mountain ranges such as the Himalayas and the Rocky Mountains.

For example, the polar jet streams—which are narrow bands of high speed winds formed by the steep temperature gradient at the polar front—owe their wave-like behaviour to this phenomena (see fig. 1).

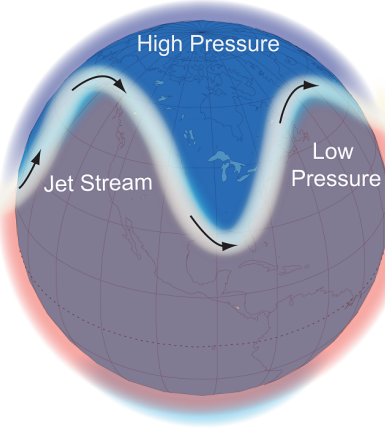


Figure 1: An illustration of the meandering of the jet stream as it passes over the Rocky Mountains and continues to oscillate around the northern hemisphere. Credit: Blunden et al., 2011, © Copyright 2017 American Meteorological Society

2 Review

2.1 Jet Streams and their Impacts on Climate

The jet streams impact daily weather as well as long term climate. For example, recent studies have shown that the polar jet stream response to vanishing Arctic sea ice appears to increase the persistence of so-called Ω -blocks, or high-pressure zones,

appearing over Greenland which may cause accelerated warming of the Greenland ice sheet (Hanna et al., 2016). During normal conditions there is a semi-permanent low-pressure system over this region which feeds the ice sheet with precipitation and keeps its rate of mass accumulation high.

Hence it is of particular interest to study the component of jet streams that is responsible for the extent of its meandering, namely the Rossby waves.

Atmospheric rivers are another weather phenomena that are still not fully understood. They are long narrow plumes of moisture in the lower troposphere that often stretch thousands of kilometers and are associated with severe flooding and precipitation events (fig. 2). These atmospheric rivers have also recently been shown to correspond to the propagation and breaking of Rossby waves in the upper troposphere such as the subtropical jet streams (Payne & Magnusdottir, 2014).

Additionally, atmospheric rivers are responsible for most of the poleward flux of moisture from the tropics and, during extreme cases, can exacerbate Arctic warming with increased cloud cover (Baggett et al., 2016). So here we can observe a possible feedback loop. Rossby waves contribute to the poleward flux of moisture via atmospheric rivers and hence increase Arctic warming. This in turn shifts the position of the highs and lows of the polar jet stream, possibly increasing the persistence of Ω -blocks over Greenland which further accelerates warming of the Greenland ice sheet. Due to the phenomena known as polar amplification—the disproportion of temperature change between the polar and temperate/tropical regions—the melting of the Greenland ice sheet then further enhances Arctic warming (Tedesco et al., 2016), and the loop continues. This may serve as a partial explanation for why current models cannot fully account for the more rapid decline of Arctic sea ice (aside from limitations in sea ice models) as external forcings are one of the most significant unknowns (Stroeve et al., 2012).

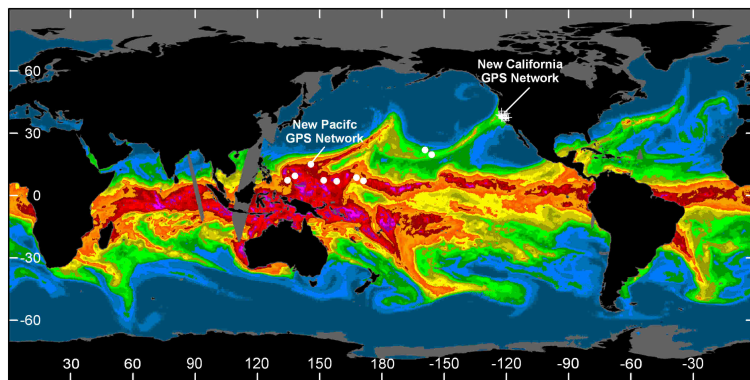


Figure 2: Satellite imagery of atmospheric rivers. Red and blue signifies high and low amounts of vertically integrated water vapour respectively. In this example we can see atmospheric rivers being 'pulled' poleward from the moisture-laden equatorial regions, possibly due to the interaction with Rossby waves in the upper troposphere as suggested by Payne & Magnusdottir, 2014. Image provided by the NOAA/OAR/ESRL PSD, Boulder, Colorado, USA, from their Web site at <https://www.esrl.noaa.gov/psd/atmrivers/resources> (public domain)

Lastly, since the Greenland ice sheet is the most significant contributor to global sea-level rise it is then imperative that we determine the intermediate mechanisms by which Arctic and Greenland warming occurs—that is, Rossby waves.

2.2 Rossby Wave Formation and Propagation

2.2.1 The Vorticity Equation

As noted earlier, Rossby waves—or more specifically orographic Rossby waves—result from conservation of potential vorticity. To determine how this quantity comes about and what it looks like, consider the horizontal momentum equations (or ageostrophic equations) for synoptic-scale flow:

$$\frac{Du}{Dt} = -\frac{1}{\rho} \frac{\partial p}{\partial x} + fv \quad (1)$$

$$\frac{Dv}{Dt} = -\frac{1}{\rho} \frac{\partial p}{\partial y} - fu, \quad (2)$$

where $\frac{D}{Dt}$ refers to the material derivative:

$$\frac{D}{Dt} = \frac{\partial}{\partial t} + \mathbf{u} \cdot \nabla, \quad \mathbf{u} = \begin{pmatrix} u \\ v \\ w \end{pmatrix},$$

and u , v , and w are the zonal, meridional, and vertical velocities respectively, ρ the density of an atmospheric column, p the average pressure of a column, and f the Coriolis parameter (also known as planetary vorticity as it is associated with circulation of winds due to Earth's rotation). By then computing:

$$\frac{\partial}{\partial x}(2) - \frac{\partial}{\partial y}(1),$$

and simplifying we ultimately arrive at the vorticity equation:

$$\frac{D}{Dt}(\zeta + f) = -(\zeta + f)(\nabla_h \cdot \mathbf{u}) - \left(\frac{\partial w}{\partial x} \frac{\partial v}{\partial z} - \frac{\partial w}{\partial y} \frac{\partial u}{\partial z} \right) - (\nabla \alpha \times \nabla p) \cdot \mathbf{k}, \quad (3)$$

where $\zeta = \left(\frac{\partial v}{\partial x} - \frac{\partial u}{\partial y} \right)$ is the relative vorticity, $\nabla_h \cdot \mathbf{u}$ the horizontal divergence of the velocity field, and $\alpha = \frac{1}{\rho}$ the reciprocal of density.

Relative vorticity is the circulation of weather systems due to curved flow or wind shear (fig. 3). It is generally positive for counter-clockwise (cyclonic) motion and negative for clockwise (anti-cyclonic) motion in the northern hemisphere (and vice versa in the southern hemisphere). Hence, at a constant latitude where f is constant, this equation describes the temporal variation of relative vorticity. Whereas if f is non-constant then it describes the temporal change in both relative and planetary vorticity (or absolute vorticity)—which refers to the vorticity of a fluid in an inertial reference frame such as Earth's axis of rotation. As such, absolute vorticity accounts for the effects of fluid motion in a rotating frame.

If we focus on the first term (the divergence term) on the right-hand side of the vorticity equation (3) we can see that the vorticity decreases for divergent flow and increases for convergent flow. And as we know, convergent flow is associated with surface lows (or cyclonic motion) whereas divergent flow is associated with surface highs (anti-cyclonic motion). So this is in-line with what we already established.

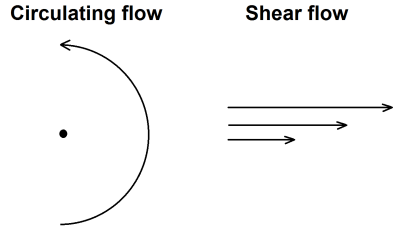


Figure 3: Both curved flow and shear flow contribute to relative vorticity.

The second term is associated with tilting or twisting of vorticity into the vertical axis. So if we have vertically tilted curved- or shear flow, this term would be important. Meanwhile, the last term corresponds to vorticity generated by pressure and density gradients. A fluid where pressure and density gradients are not aligned is called a baroclinic fluid (fig. 4).

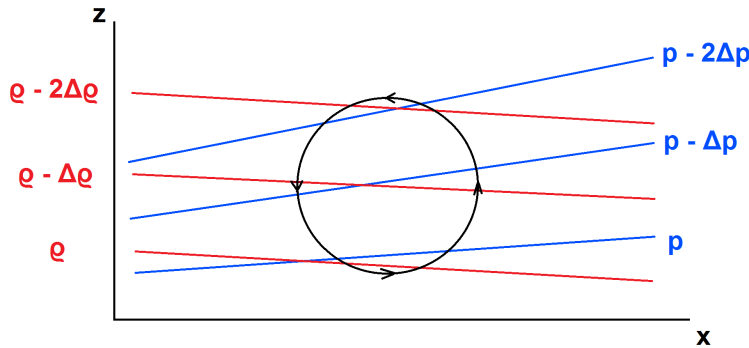


Figure 4: An example of a baroclinic front with cold air sinking on the left (behind the front) and warm air rising on the right (ahead of the front). When surfaces of constant pressure are not aligned with surfaces of constant density these will try to realign, and in doing so they generate horizontal/absolute vorticity. This is why baroclinic fronts are associated with more frequent formation of cyclones.

In contrast, in a barotropic fluid the pressure and density gradients are already aligned, which is equivalent to saying that density only depends on pressure and not temperature. This is the case we'll be focusing on as it simplifies the vorticity equation (3) to just the divergence term and the horizontal material derivative ($\frac{D_h}{Dt}$) of the vorticity (the material derivative without the vertical component):

$$\frac{D_h}{Dt}(\zeta + f) = -(\zeta + f)(\nabla_h \cdot \mathbf{u}) \quad (4)$$

This assumption limits us to only looking at the orographic component of the jet streams since they form due to a variety of factors, such as the steep temperature gradient at the polar front (NOAA/NWS, [n.d.](#)). As highlighted in the vorticity equation, these gradients generates additional vorticity.

2.2.2 Barotropic Potential Vorticity Conservation

Now we want to simplify the vorticity equation even further in order to understand it and apply it. Consider a homogeneous, incompressible fluid ($\rho = \text{const.}$). The continuity equation (5) then yields $\nabla \cdot \mathbf{u} = 0$.

$$\frac{\partial \rho}{\partial t} = -\nabla \cdot (\rho \mathbf{u}) \quad (5)$$

So we get that the horizontal divergence is equivalent to the vertical acceleration:

$$\frac{\partial u}{\partial x} + \frac{\partial v}{\partial y} = \nabla_h \cdot \mathbf{u} = -\frac{\partial w}{\partial z}. \quad (6)$$

We now substitute this into the vorticity equation to get:

$$\frac{D_h}{Dt}(\zeta + f) = (\zeta + f)\frac{\partial w}{\partial z}.$$

For purely horizontal flow ($w = 0$) we then get conservation of absolute vorticity:

$$\frac{D_h}{Dt}(\zeta + f) = 0. \quad (7)$$

For example consider a fluid parcel moving north from the equator. This will increase f and thus ζ will have to decrease in order for conservation of absolute vorticity to hold. For a more generalized view, again assume a homogeneous, incompressible fluid:

$$\frac{D_h}{Dt}(\zeta + f) = (\zeta + f)\frac{\partial w}{\partial z},$$

and then integrate vertically from the heights z_1 to z_2 :

$$\frac{D_h}{Dt}(\zeta + f) = (\zeta + f)\frac{w(z_2) - w(z_1)}{z_2 - z_1}.$$

We define the layer thickness $h = z_2 - z_1$, and since:

$$w(z_2) - w(z_1) = \frac{z_2 - z_1}{t_2 - t_1} = \frac{\partial h}{\partial t} = \frac{D_h h}{Dt}, \quad (8)$$

we have that:

$$\frac{1}{(\zeta + f)} \frac{D_h}{Dt}(\zeta + f) = \frac{1}{h} \frac{D_h h}{Dt}.$$

By integrating both sides by Dt and differentiating by Dt again we get:

$$\frac{D_h}{Dt} \ln(\zeta + f) = \frac{D_h}{Dt} \ln h.$$

Moving the right-hand side over to the left side and using a logarithm property we get:

$$\frac{D_h}{Dt} \ln \left(\frac{\zeta + f}{h} \right) = 0.$$

If the logarithm of a quantity is conserved then the quantity inside the logarithm also has to be conserved, so ultimately we find that:

$$\frac{D_h}{Dt} \left(\frac{\zeta + f}{h} \right) = 0. \quad (9)$$

If we let $w = 0$ then h is constant and we get back to (7).

The conserved quantity inside the brackets is called the *barotropic potential vorticity* q of a fluid column:

$$q = \frac{\zeta + f}{h} = \text{const. } [\text{m}^{-1}\text{s}^{-1}] \quad (10)$$

Thus, barotropic potential vorticity is conserved following a fluid column and measures the absolute vorticity relative to the depth of the vortex. This is the basis for Rossby-wave formation. For example, consider a fluid column moving over topography. Since at any given latitude the Coriolis parameter is constant, the only parameter that can change in response to a change in thickness is the relative vorticity (fig. 5).

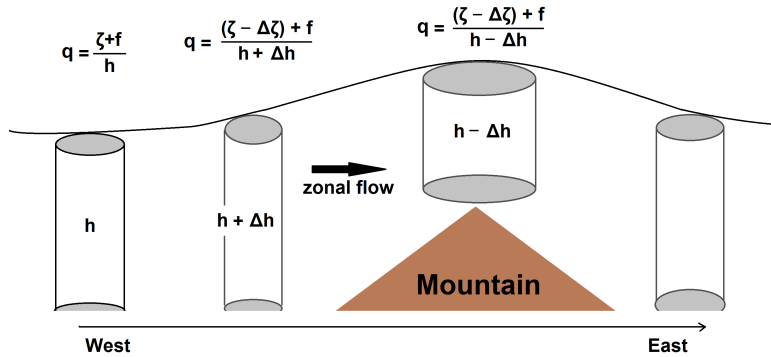


Figure 5: In order for potential vorticity to be conserved within a fluid as it moves zonally, the relative vorticity has to increase as it approaches the vicinity of a mountain (due to the fluid layer increasing in height before the mountain). As such, the fluid will be redirected to the north in the northern hemisphere. As it flows over the mountain however, the fluid depth decreases again, and consequently the relative vorticity decreases.

For very large mountain ranges such as the Rocky Mountains the planetary vorticity (Coriolis parameter) also varies. For example, as seen in a top-down view (fig. 6) similar to the previous scenario, as the fluid is deflected north to higher latitudes before reaching the mountain its planetary vorticity increases along with the layer thickness. The layer thickness then rapidly starts decreasing as the fluid columns start passing over the mountain. In accordance with this, the relative vorticity has to decrease in order to conserve potential vorticity, and we see the fluid being deflected back towards the south again. The fluid then reaches the southernmost point with a momentum ‘overshoot’ and hence keeps oscillating back and forth despite no further

change in topography elevation—mimicking a tug of war between relative vorticity and planetary vorticity.

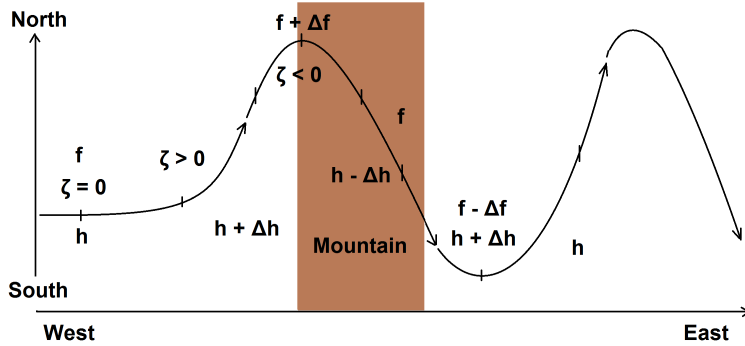


Figure 6: Top-down view of fig. 5.

2.3 The Global-Scale Shallow Water Equations

The shallow water equations (SWEs), which are a set of hyperbolic partial differential equations (PDEs), essentially describes the surface of any incompressible, inviscid fluid but can be used to model many different scenarios—including large-scale ocean- and atmospheric circulation—so long as the horizontal length scales are much greater than the vertical length scales in addition to vertical velocities being negligible. Note that there are multiple assumptions made implicitly in the following segments. Warner, 2011 covers these in great detail and is a highly recommended read.

2.3.1 Shallow Water Continuity Equation

First, consider an infinitesimal shallow fluid parcel/column in two dimensions, which flows barotropically, whose fluid depth (or thickness) at any position (x, y) at a time t is $h(x, y, t)$ (fig. 7). Also assume it's incompressible. Applying the continuity equation (5) to this parcel, we then have:

$$\frac{\partial \rho}{\partial t} = -\nabla \cdot (\rho \mathbf{u})$$

↓

$$\nabla \cdot \mathbf{u} = 0$$

By integrating this equation from the bottom B to the top of the layer $B + h$ (recalling from (8) that $w(B + h) - w(B) = \frac{\partial h}{\partial t}$ and that the vertically integrated horizontal divergence is equivalent to the vertical velocity (6)) we get:

$$\begin{aligned} 0 &= \int_B^{B+h} \left(\frac{\partial u}{\partial x} + \frac{\partial v}{\partial y} \right) dz + w(B+h) - w(B) \\ &= \frac{\partial}{\partial x} \int_B^{B+h} u dz + \frac{\partial}{\partial y} \int_B^{B+h} v dz + \frac{\partial h}{\partial t} \end{aligned}$$

Since the fluid is assumed to be shallow (fig. 8) we can assume the horizontal velocities to be constant with depth (also neglecting shear forces like the no-slip condition which only applies in the boundary layer). The depth-integrated velocities then simplify ($\int_B^{B+h} u dz = hu$, etc.) and we get:

$$\frac{\partial h}{\partial t} + \frac{\partial(hu)}{\partial x} + \frac{\partial(hv)}{\partial y} = 0. \quad (11)$$

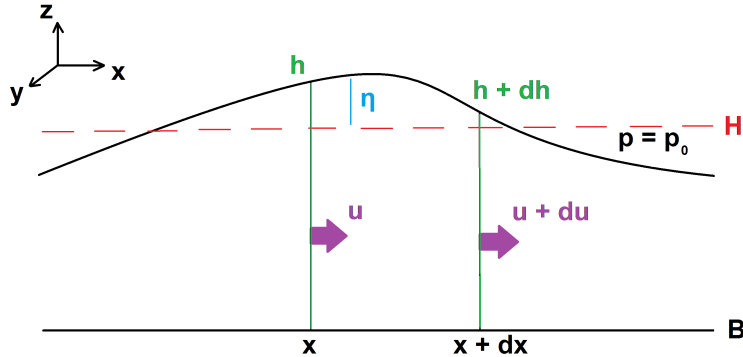


Figure 7: A shallow fluid parcel where vertical motions are neglected and horizontal velocities are depth-averaged. Here, h is the layer thickness, H the average layer thickness, and η the displacement from the average thickness such that $h(x, y, t) = H(x, y) + \eta(x, y, t)$. So it then follows that $\frac{\partial h}{\partial t} = \frac{\partial \eta}{\partial t}$. Lastly, B is the height of topography (0 in this case), and p_0 the pressure at the surface layer which is assumed to be negligible.

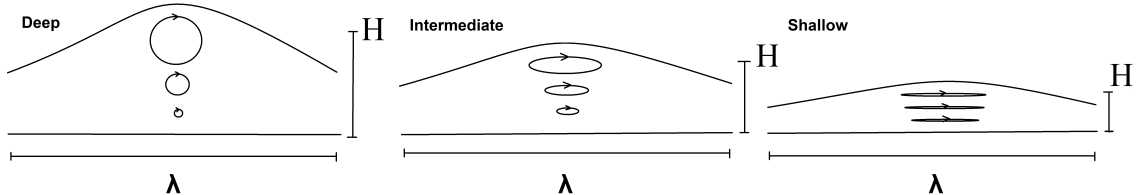


Figure 8: Here we have the more quantitative definition of "shallow water". When the ratio of fluid depth H and the wavelength λ is $\frac{H}{\lambda} > \frac{1}{2}$ it is considered deep. If however $\frac{H}{\lambda} < \frac{1}{20}$ it is considered shallow since vertical motion largely becomes negligible at this point, which implies that we can accurately utilize the SWEs.

2.3.2 Curvature, and Potential Vorticity in the Shallow Water Momentum Equations

The momentum equations for shallow water take the same form as the ageostrophic equations (1 and 2). However, for large-scale motion where the characteristic length scale is 10,000 km or more we need to account for Earth's curvature (as determined by using scale analysis). The additional terms for curvature/geometry naturally pop up when deriving the Coriolis momentum terms and are here added back into (1) and (2), which yields:

$$\begin{aligned}\frac{D_h u}{Dt} + \frac{1}{\rho} \frac{\partial p}{\partial x} &= f v + \frac{u v \tan \phi}{a} \\ \frac{D_h v}{Dt} + \frac{1}{\rho} \frac{\partial p}{\partial y} &= -f u - \frac{u^2 \tan \phi}{a},\end{aligned}$$

where ϕ is the latitude and a is Earth's radius. Expanding the material derivatives and utilizing the hydrostatic approximation:

$$p = \rho g(\eta - z) \implies \frac{\partial p}{\partial x} = \rho g \frac{\partial \eta}{\partial x},$$

and lastly putting these together with (11) we get our closed system of equations:

$$\frac{\partial h}{\partial t} + \frac{\partial(hu)}{\partial x} + \frac{\partial(hv)}{\partial y} = 0 \quad (12)$$

$$\frac{\partial u}{\partial t} + u \frac{\partial u}{\partial x} + v \frac{\partial u}{\partial y} + g \frac{\partial \eta}{\partial x} = f v + \frac{u v \tan \phi}{a} \quad (13)$$

$$\frac{\partial v}{\partial t} + u \frac{\partial v}{\partial x} + v \frac{\partial v}{\partial y} + g \frac{\partial \eta}{\partial y} = -f u - \frac{u^2 \tan \phi}{a}. \quad (14)$$

Although potential vorticity is implicitly conserved in the SWEs (or rather q does not change significantly), we can still use conservation of potential vorticity to simplify the system by explicitly setting $q = \text{constant}$. First, however, we need to rewrite the system to accommodate this. Recalling that $\zeta = \left(\frac{\partial v}{\partial x} - \frac{\partial u}{\partial y} \right)$, we can use the product rule in reverse to find that:

$$\begin{aligned}u \frac{\partial u}{\partial x} + v \frac{\partial u}{\partial y} &= \frac{\partial K}{\partial x} - \zeta v \\ u \frac{\partial v}{\partial x} + v \frac{\partial v}{\partial y} &= \frac{\partial K}{\partial y} + \zeta u,\end{aligned}$$

where $K = \frac{1}{2}(u^2 + v^2)$ is the kinetic energy density. When substituting these equations into (12-14), and rewriting ζ as $\zeta = hq - f$ from (10) we find that the Coriolis terms cancel out. After collecting the derivative terms we ultimately end up with the following system:

$$\begin{pmatrix} h \\ u \\ v \end{pmatrix}_t + \begin{pmatrix} hu \\ K + gn \\ 0 \end{pmatrix}_x + \begin{pmatrix} hv \\ 0 \\ K + gn \end{pmatrix}_y = \begin{pmatrix} 0 \\ hq v + \frac{1}{a} u v \tan \phi \\ -hqu - \frac{1}{a} u^2 \tan \phi \end{pmatrix}, \quad (15)$$

where subscripts denote derivatives. This system governs shallow large-scale barotropic flow which is suitable for many processes in the atmosphere, including simulation of orographic Rossby waves. It may also be written in compact vector form as:

$$U_t + F(U)_x + G(U)_y = S(U). \quad (16)$$

where:

$$F(U) = \begin{pmatrix} hu \\ K + gn \\ 0 \end{pmatrix}, \quad G(U) = \begin{pmatrix} hv \\ 0 \\ K + gn \end{pmatrix}, \text{ and } S(U) = \begin{pmatrix} 0 \\ hq\nu + \frac{1}{a}uv \tan \phi \\ -hqu - \frac{1}{a}u^2 \tan \phi \end{pmatrix}.$$

This form is also known as a hyperbolic conservation law. It can be integrated over a volume and rewritten using the divergence theorem which highlights that F and G are momentum fluxes at the boundary of the volume (in this case our fluid parcel) whereas U is the change in momentum inside the parcel and S accounts for external sources of momentum.

Although we cannot write F , G , and S explicitly as functions of U we will find later on that we can still write them in terms of the elements of U which is how we're going to solve the system. If we could not write F , G , and S in terms of the elements of U then our attempts at solving the system in the next sections would be futile.

Through the process of linearization of the SWEs—which have been omitted from this paper—we find that the maximum allowable velocities in x and y are $u \pm \sqrt{gh}$ and $v \pm \sqrt{gh}$ respectively. This will be important for the stability of the numerical methods in the next couple of sections.

2.4 Numerical Techniques

Due to their complexity, there are no general analytical solutions to the SWEs and as such we need to resort to numerical techniques. In this project we're employing finite difference schemes (FDSs) which use truncated Taylor series approximations for derivatives and solves the PDEs on a finite grid. For example, here we have a couple of finite difference (FD) approximations:

$$\text{Forward-difference in time: } \frac{\partial U}{\partial t} = \frac{U_{i,j}^{n+1} - U_{i,j}^n}{\Delta t}$$

$$\text{Backward-difference in } x: \frac{\partial U}{\partial x} = \frac{U_{i,j}^n - U_{i-1,j}^n}{\Delta x}$$

$$\text{Central-difference in } y: \frac{\partial U}{\partial y} = \frac{U_{i,j+1}^n - U_{i,j-1}^n}{2\Delta y}.$$

In this context the roman subscript indices refer to the position in space, where i refers to the x -position $i\Delta x$ whereas j refers to the y -position $j\Delta y$ in the grid. Similarly, the superscript n is the time index for the time $n\Delta t$. So e.g. when we write $U_{1,2}^3$ that's the value of U at the grid position $\{1, 2\}$ at the time index 3. By substituting these FD approximations into PDEs we can approximate their solutions at the grid. (see fig. 9)

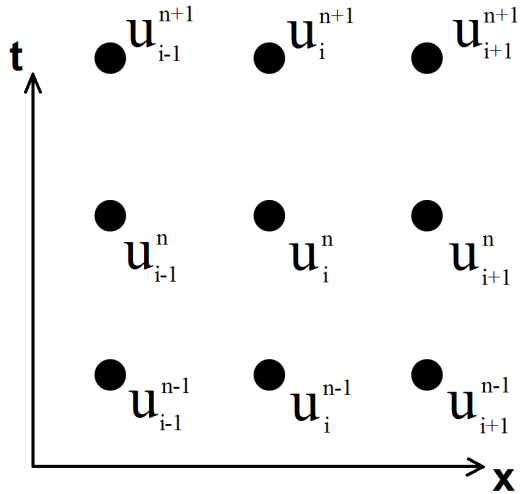


Figure 9: A finite difference grid with one spatial dimension and one time dimension.

2.4.1 The Forward-Time Central Space Scheme

Before heading into the more complex FDSs that are commonly used to solve the SWEs we need to go through the more basic ones first by which they are built upon which, in addition, also highlights the issue of stability that we have to take into consideration later.

The Forward-Time Central-Space (FTCS) scheme uses—as its name suggests—a forward difference approximation for the time derivatives and central differences for the spatial derivatives. Although this scheme generally works fine for parabolic PDEs, it is inherently unstable for hyperbolic PDEs such as the SWEs.

A simpler hyperbolic PDE is the one-dimensional advection equation which simply models the transport of some substance or conserved property by a fluid with the velocity c :

$$\frac{\partial U}{\partial t} + c \frac{\partial U}{\partial x} = 0.$$

If we substitute the forward difference for the time derivative and the central difference for the spatial derivative we find that:

$$\begin{aligned} \frac{U_i^{n+1} - U_i^n}{\Delta t} + c \frac{U_{i+1}^n - U_{i-1}^n}{2\Delta x} &= 0 \\ \downarrow \\ U_i^{n+1} &= U_i^n - \frac{c\Delta t}{2\Delta x} (U_{i+1}^n - U_{i-1}^n) + \mathcal{O}(\Delta t, \Delta x^2) \end{aligned}$$

This is the FTCS scheme for the advection equation which is 1^{st} -order accurate in time and 2^{nd} -order accurate in space. However as stated, it is unconditionally unstable, which means that it is unstable for all values of Δt . That is, if we try to solve the equation using this method minor oscillations will quickly grow to infinity and ‘blow up’ the solution—making it effectively useless.

2.4.2 Convergence, Consistency, and Stability

There are a number of conditions that needs to be satisfied in order for a FDS to converge to a solution and not blow up. In order for a FDS to converge to the actual solution the approximation should improve as $\Delta t, \Delta x \rightarrow 0$, i.e. the error $\epsilon = U_{true} - U_{approx}$. should approach zero as $\Delta t, \Delta x \rightarrow 0$. The Lax Equivalence Theorem states that a scheme is convergent if it is both *consistent* and *stable*.

Consistency can be shown by replacing the U_i^n terms with the corresponding Taylor series expansions and then rearranged to the form of the PDE. If the leftover terms—i.e. the truncation error—tend to zero as $\Delta t, \Delta x \rightarrow 0$, then the scheme is consistent. Similarly, a scheme is said to be stable if the sequence of errors as $t \rightarrow \infty$ remains bounded—i.e. the error does not grow exponentially with time.

The CFL Condition

With time-marching schemes, the larger Δt is, the less time steps are required for the full solution over a time interval. However, using too large Δt may cause the scheme to become unstable as highlighted previously. For explicit schemes, which we're using here, there is generally a limit to the value of Δt for which it is stable—called the Courant-Friedrichs-Lowy (CFL) condition. The CFL condition has to be satisfied in order for a scheme to be stable, but just because it is satisfied *doesn't* mean that the scheme is stable.

The CFL condition states that the physical domain of dependence must be contained within the numerical domain of dependence. Essentially, this is saying that in one time step Δt the fastest waves cannot travel further than the distance Δx . I.e. $|c| \Delta t \leq \Delta x$ has to be satisfied in order for the motion to be captured in the approximation. We can rearrange this condition into:

$$C = \frac{|c| \Delta t}{\Delta x} \leq 1 \implies \Delta t \leq C \frac{\Delta x}{|c|}$$

where C is the so-called Courant number, which will be a constant we set to a stable number for a given scheme. We never set our Δt exactly equal to the limit however because of rounding errors in computers. E.g. if the limit is 1 and we set our $\Delta t = 1$ then the computer may round it as $\Delta t = 1.000\dots001$, making it unstable.

Normally if we were doing a simulation that might take weeks or more (where we would want to save as much computation time as possible) we would go through the process of determining the value of the Courant number for our scheme using what's called von Neumann stability analysis which involves a bit of Fourier analysis. However for this project we can just pick a low enough Δt so that our scheme remains stable without sacrificing much time. The finding from such an analysis on the FTCS scheme shows that the only stable value for Δt is zero for the advection equation, which means that it is unconditionally unstable.

2.4.3 The Lax-Friedrichs Scheme

The Lax-Friedrichs (LF) scheme attempts to stabilize the FTCS scheme for hyperbolic PDEs by using a central difference for spatial- and a corrected forward difference for time derivatives. The correction is that the U_i^n term is replaced by an average of the

two terms next to it $\frac{1}{2}(U_{i-1}^n + U_{i+1}^n)$. If we were using the 2D advection equation we would take the average of the four neighboring spatial terms. The resulting scheme for the 1D advection equation is as follows and its node dependencies are highlighted in figure 10.

$$U_i^{n+1} = \frac{1}{2}(U_{i+1}^n + U_{i-1}^n) - \frac{c\Delta t}{2\Delta x}(U_{i+1}^n - U_{i-1}^n) + \mathcal{O}(\Delta t, \Delta x).$$

Some von Neumann stability analysis shows that this small change makes the FTCS scheme conditionally stable (i.e. stable for specific values of Δt), but at a reduced order of accuracy in the spatial domain.

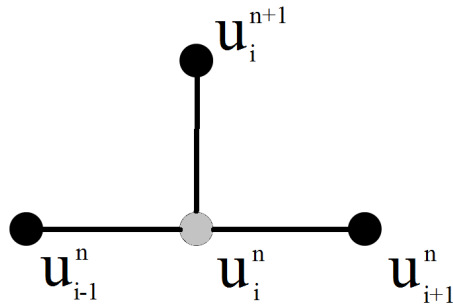


Figure 10: A stencil, showcasing the dependencies in the LF scheme. Greyed out nodes are nodes that aren't used. The FTCS scheme used the central node U_i^n as well as U_{i+1}^n and U_{i-1}^n whereas the LF scheme removes the dependency on U_i^n —making the scheme conditionally stable at least.

2.4.4 The Leapfrog Scheme

The Leapfrog scheme uses a central difference for both time- and spatial derivatives. The name comes from the fact that the scheme "leapfrogs" above the node U_i^n as can be seen in figure 7. However, since the scheme depends on an earlier time step $n - 1$ we need to use another scheme to calculate the first step U_i^1 in order to kick-start the Leapfrog scheme. This scheme has an order of accuracy of $\mathcal{O}(\Delta t^2, \Delta x^2)$.

2.4.5 The Lax-Wendroff Scheme

Ultimately, we arrive at our scheme of choice for solving the SWEs. The Lax-Wendroff (LW) scheme is a two-stage process where the first stage uses the LF scheme as a *predictor* and the second stage uses the Leapfrog scheme as a *corrector*. As seen in figure 12, the LF scheme is used twice to calculate the solution for two nodes at half time steps (4 nodes in the 2D case). These nodes are then used by the Leapfrog scheme to calculate the value at the next time step U_i^{n+1} .

This scheme looks like the FTCS scheme—in that its core dependencies are U_{i-1}^n , U_i^n , and U_{i+1}^n —but it is conditionally stable and has an order of accuracy of $\mathcal{O}(\Delta t^2, \Delta x^2)$. Also, unlike the some of the other schemes we've shown, it exhibits no dissipation—which is the tendency of sharper curves to flatten out with time

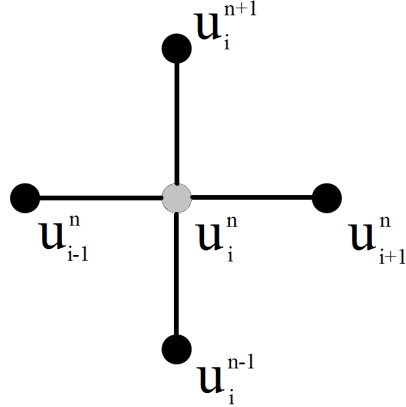


Figure 11: Stencil for the Leapfrog scheme, highlighting node dependencies.

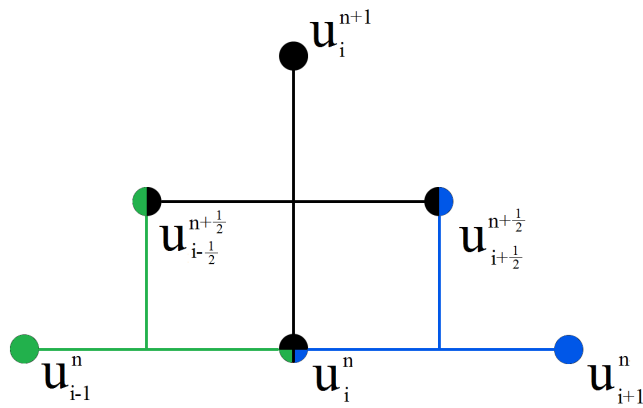


Figure 12: Stencil for the LW scheme. Two uses of the LF scheme are employed to calculate the intermediate prediction values at $U_{i+\frac{1}{2}}^{n+\frac{1}{2}}$ and $U_{i-\frac{1}{2}}^{n-\frac{1}{2}}$ respectively (highlighted in green and blue). The final correction method then employs the Leapfrog scheme in the middle (highlighted in black) to calculate the final correction value U_i^{n+1} .

inadvertently which may be problematic when dealing with e.g. waves with sharp profiles (like gravity waves when running simulations on a planetary scale).

2.4.6 Boundary Conditions

In order to implement boundary conditions (BC:s) on a finite grid we need to have extra nodes outside our domain of interest. These are sometimes termed ‘ghost nodes’, or ‘ghost points’ (fig. 13).

If we were looking at water waves in a bath tub we would have reflective boundary conditions which, for the SWEs, take the form:



Figure 13: Ghost nodes such as U_{-1} here are used to enforce boundary conditions.

$$\begin{aligned} h_{-1} &= h_1 \\ h_{N+1} &= h_{N-1} \\ u_{-1} &= -u_1 \\ u_{N+1} &= -u_{N-1}, \end{aligned} \tag{17}$$

where $i = 0$ and $i = N$ are the outermost nodes within the domain and $i = -1$ and $i = N + 1$ are the ghost nodes.

Meanwhile, if we want transient flow boundary conditions (i.e. any waves reaching the boundaries just flow out of it) we just set zero gradient across the boundary (a subset of Neumann boundary conditions):

$$\begin{aligned} h_{-1} &= h_1 \\ h_{N+1} &= h_{N-1} \\ u_{-1} &= u_1 \\ u_{N+1} &= u_{N-1}. \end{aligned} \tag{18}$$

We can also have periodic boundary conditions which simply just means that whatever comes out one end continues at the other end of the domain:

$$h_{-1} = h_{N+1}$$

Lastly, we have pinned boundary conditions (a subset of Dirichlet boundary conditions) where e.g. h is just set to a constant.

3 Methodology

To model the problem we use MATLAB® (details in ch. 7). We'll go through the overall structure of the code here but will leave out some numerical details. The full code is provided as supplemented material.

Before we start solving (16) we define our computational domain and parameters (detailed in appendix B.1).

3.1 Orography and β -Plane Approximation

We now need to add some preliminary boundary conditions. In this case we're starting off with a simple Gaussian-curve-shaped mountain as topography, however

we may define B ourselves or use the inbuilt world topography data set in MATLAB (fig. 14). This dataset is sharp and fairly discontinuous however which can induce instabilities in the numerical schemes. So we apply a smoothing function to the topography before using it for any simulation (fig 15). Here we also interpolate the data to fit our domain (see appendix B.2 for details).

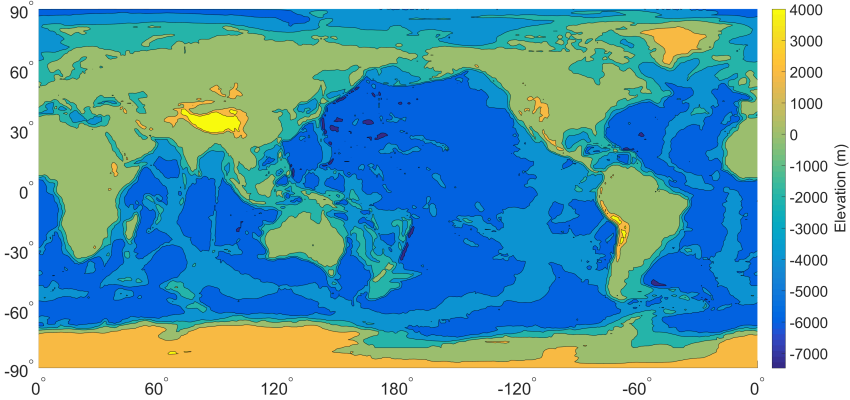


Figure 14: The inbuilt topographical dataset in MATLAB comes from the ETOPO1 Global Relief Model by NOAA and is used in our model as orography.

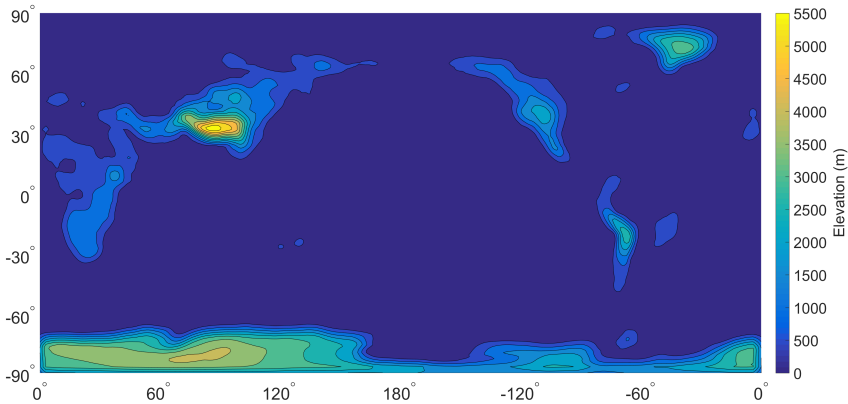


Figure 15: Corrected and smoothed data that still encapsulates the important topographical features that generate large-scale Rossby waves.

In addition to this, we have to define the Coriolis parameter and how it varies in space. The Coriolis parameter ($f = 2\Omega \sin \phi$) is a curved plane that varies non-linearly in y —since it depends on the sine of the latitude. Because of this, it is prone to stability issues as non-linear terms tend to cause so-called numerical phase errors. By linearizing the f -plane we can avoid the brunt of such issues. This is done using the so-called β -plane approximation which linearizes f as follows (fig. 16). We define f_0 as:

$$f_0 = 2\Omega \sin \phi_0,$$

where ϕ_0 is a latitudinal degree close to the region of interest. We then define β as the linear coefficient (constant slope) of the f -plane which is given by:

$$\beta = \frac{2\Omega \cos \phi_0}{a}.$$

The linear approximation of f is then given by:

$$f = f_0 + \beta(y - \bar{y}),$$

where \bar{y} is the average of y . These steps are mirrored as code in appendix B.3.

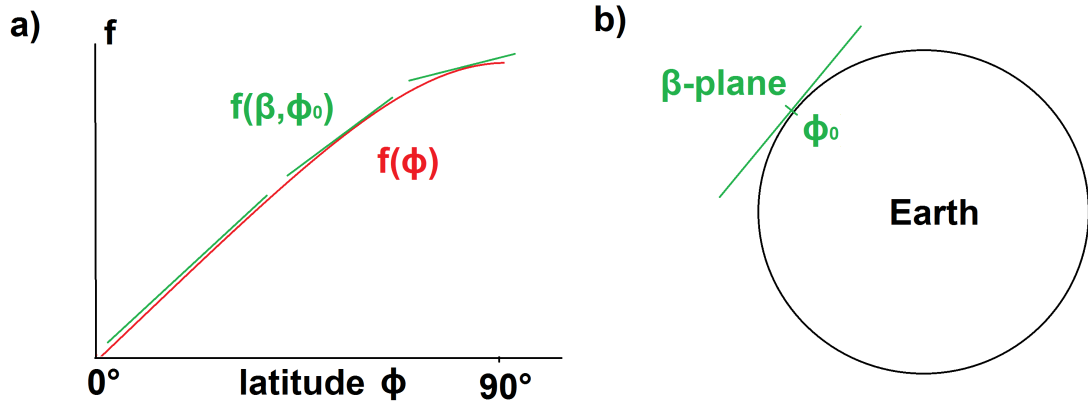


Figure 16: **a)** Schematic of non-linear f -plane (red) and a variety of β -plane approximations (green) for various spans of latitude. **b)** ϕ_0 is chosen at the mid plane of the region of interest. This figure also highlights the relative error of the approximation as the fluid strays from ϕ_0 . A single β -plane approximation would be fairly useless if doing a global simulation from -90° to 90° for example. Hence, in this project we'll stick to smaller latitude spans of a few dozen degrees at most.

3.2 Initial Conditions

Our initial conditions are idealized. The layer thickness h for example is assumed to have a linear profile from south to north. This will generate the pressure-gradient force responsible for upholding the geostrophic balance along with the Coriolis effect. The vector U in (16) is denoted as a 3D matrix where the rows and columns denote spatial indices (j for rows and i for columns) and the pages of the matrix (the 3rd dimension of the matrix) denotes the variable. So page 1 represents h , page 2 u , and page 3 v (i.e. $U(j, i, 1) = h$, $U(j, i, 2) = u$, etc.). See appendix B.4 for details.

Our initial conditions for the velocity-field will be a geostrophic wind balance, that is:

$$u_g = -\frac{g}{f} \frac{\partial h}{\partial y}$$

$$v_g = \frac{g}{f} \frac{\partial h}{\partial x}.$$

Lastly, we assume zero initial vorticity in the field which means $\zeta_{i,j}^{n=1} = 0$, and hence

$q_{i,j} = \frac{f_{i,j}}{h_{i,j}^n}$ from (10). That is, the initial potential vorticity will remain constant for all time and is initially determined by $\frac{f}{h}$. These are computed in MATLAB as detailed in appendix B.4.1.

3.3 Solving the System of Equations

With the boundary- and initial conditions established we start entering the loop that solves the system. Starting at $n = 1$ we iterate until the time t_{max} has been reached. At each step we calculate the maximum velocity and adapt the time step accordingly in order to uphold stability. This follows the same principle as reviewed in ch. 2.4.2. Lastly, one step of the LW method is computed, followed by an update in time in preparation for the solution at the next time step (appendix B.5)

Finally, the Lax-Wendroff (LW) scheme solves our system (16) for one time step. It is implemented as follows. Since this is in two dimensions it can be a bit confusing but it's the same principle as showcased previously in ch. 2.4.5. Recall that we have:

$$U_t = F(U)_x + G(U)_y = S(U).$$

We start off by calculating 4 half steps in time ($n + \frac{1}{2}$) using the Lax-Friedrich (LF) method for the nodes $U_{i+\frac{1}{2},j}^{n+\frac{1}{2}}$, $U_{i-\frac{1}{2},j}^{n+\frac{1}{2}}$, $U_{i,j+\frac{1}{2}}^{n+\frac{1}{2}}$, and $U_{i,j-\frac{1}{2}}^{n+\frac{1}{2}}$. The LF steps are highlighted in figure 17a. Unlike in the LW example given previously, here we're calculating the spatial derivatives of F and G instead of just U for the LF steps. However, if we know U then we can easily obtain F and G via (15).

For the next step we use the Leapfrog scheme which requires $F_{i\pm\frac{1}{2},j}^{n+\frac{1}{2}}$ and $G_{i,j\pm\frac{1}{2}}^{n+\frac{1}{2}}$ which are simply obtained from the previously calculated $U_{i\pm\frac{1}{2},j}^{n+\frac{1}{2}}$ and $U_{i,j\pm\frac{1}{2}}^{n+\frac{1}{2}}$ (fig. 17b). These steps are detailed in appendix B.6.

4 Results and Discussion

We run a variety of trials to validate and stress test the model. For example, since these are the shallow water equations they should be able to fairly accurately model shallow water. This is the subject of the first set of trials in ch. 4.1 where large-scale features such as Coriolis and Earth curvature are neglected and we observe how water waves behave in a bathtub.

Unfortunately our implementation of the model does not appear to be stable on large scales with Coriolis, orography, and curvature. Instead we utilize a previous model by Hogan, n.d—which solves the traditional equations (12-14)—and make some heavy modifications to it in order for it to suit our own model. This model also uses the Lax-Wendroff method, albeit with a couple of corrections as detailed in the source code. However, for inexplicable reasons, even this method is unstable for our set of equations, so we ultimately rewrite it to use a simpler dimensionally split Lax-Friedrich method instead (see appendix A.1 and B.8). This method is stable, but has a much worse order of accuracy, $\mathcal{O}(\Delta x, \Delta y, \Delta t)$, which impacts the final results.

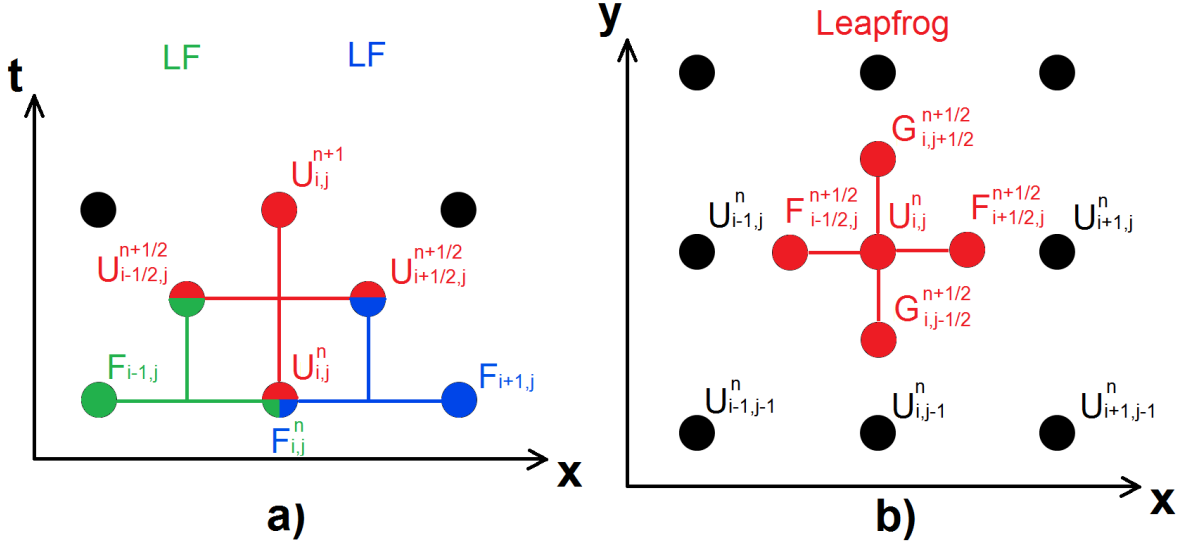


Figure 17: a) The LF scheme is used to calculate U at four different spatial positions— $(i \pm \frac{1}{2}, j)$ and $(i, j \pm \frac{1}{2})$ —at a half time step $(n + \frac{1}{2})$. b) In the next step, these half-steps are used to calculate the F and G at the same positions. These are then used in the Leapfrog scheme to calculate U at (i, j) for the full time step $(n + 1)$

4.1 Effects of Artificial Viscosity

If we run our model without any Coriolis effect, topography, curvature, or geostrophic conditions and instead simulate a water droplet in a bathtub with reflective boundaries (Gaussian curve test) we find that large wavenumber (high-frequency) waves start to oscillate with larger and larger amplitude as time moves on (fig. 18). As noted by Hudson, 2001, this is expected due to numerical phase- and aliasing errors. However, it can be remedied by introducing artificial viscosity which dampens small waves. Implementing real molecular viscosity is difficult since it acts on a much smaller scale and cannot be resolved by the typical mesh grid. Hence, it has to be parameterized (Tan, 1992).

To remedy this, at the end of the Lax-Wendroff scheme we add additional terms accordingly with Tryggvason, 2011 that replicate viscosity (see appendix A.2). Although this adds significant extra computational cost, it is necessary when we have lots of relatively high-frequency waves (such as gravity waves) in order to keep them from growing exponentially in amplitude. The result of adding this can be seen in fig. 19.

4.2 Orographic Rossby Waves

Replicating the boundary- and initial conditions of the real atmosphere is a daunting task. Hence, the following results are merely idealized solutions that encapsulate some general behaviours in the atmosphere. That is, the results are for more diagnostic purposes and are still preliminary (subject to large errors). With these caveats established, our boundary conditions in the trials henceforth are employed in appendix B.7 (see ch. 2.4.6 for the definitions of transient, reflective, pinned, and periodic boundary conditions).

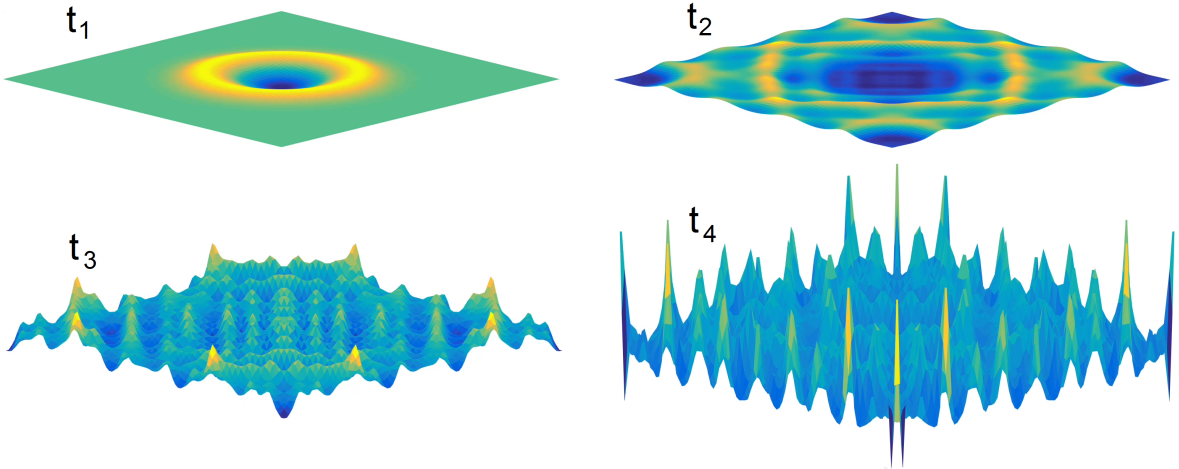


Figure 18: In a bathtub scenario the small waves generated from a droplet at t_1 start to amplify as they're reflected off the walls (t_2-t_3) and ultimately end up amplifying towards infinity (t_4).

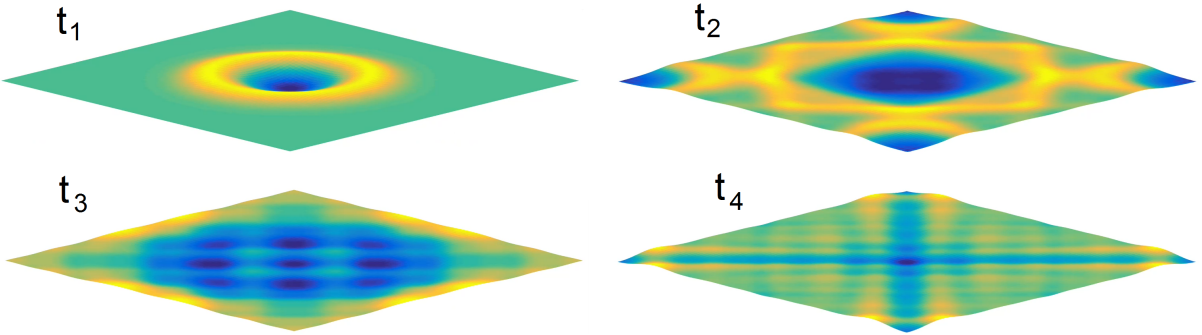


Figure 19: With a viscosity coefficient of $D = 1$ (as defined in Tryggvason, 2011, small waves do not grow in amplitude with time but are still not fully dissipated. For $D = 5$ they almost completely dissipate after a while (not showcased here)).

Despite numerous issues with stability and the high sensitivity of boundary conditions and initial conditions we find that wave-like behaviours in the mid-high-troposphere are somewhat generated, similar to that of planetary-scale Rossby waves (figs. 20, 21). However these do not appear to behave the same way as discussed in ch. 2.2.2. Figure 20 showcases the evolution of these waves from the initial conditions. The initial conditions generate low pressure zones over all the continents and these fade with time. Ultimately we end up with an equilibrium where we can only observe slight dips in pressure around the lee sides of the high orographies of the Tibetan Plateau and Rocky Mountains. This is partially expected from the overall trends of semi-permanent pressure zones during summer months (July) (see appendix C.1). Unlike discussed in ch. 2.2.2 however we do not see any increase in relative vorticity (ζ) on the windward sides of the mountain ranges and the subsequent reduction in ζ as the winds move north. Instead we see the increase in ζ on the lee sides of the mountain ranges and the subsequent decrease thereafter. So although the model can replicate some of the large-scale features of the atmosphere, it is still very primitive and requires extensive work in order to be useful for even diagnostic purposes such as assessing the overall impacts of Rossby waves on

climate.

At closer inspection, the fluid surface simply doesn't flatten out enough in accordance with figure 5 which is likely the culprit of the lack of generation of ζ on the windward sides of the mountain ranges. Yet at the same time, due to the low order of accuracy, the Lax-Friedrich method dampens the waves too much to generate larger variations in the meanders as can be seen by the same results in the model by Hogan, n.d (fig. 22).

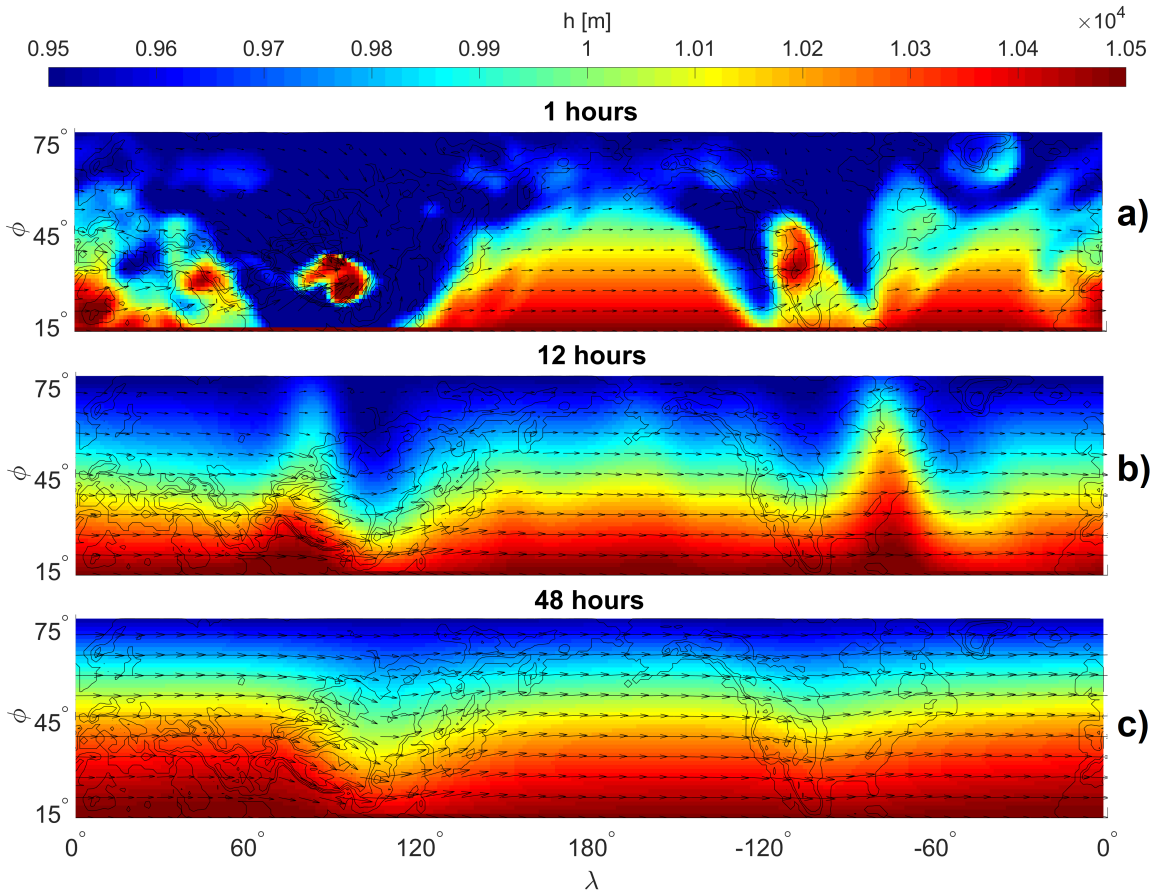


Figure 20: Northern hemisphere pressure and velocity field distribution. The colorbar represents the layer thickness or depth (pressure) distribution h and arrows represent the depth-averaged wind vectors. Contours represent orography levels at increments of $\{1, 5e2, 1e3, 2e3, 3e3, 5e3\}$ m. **a)** Initial layer thickness distribution at geostrophic balance. **b)** Around the first couple of hours meandering in the pressure field occurs but not the velocity field, likely due to the excess of gravity waves generated at initialization as the fields adjust to an ageostrophic equilibrium. **c)** At equilibrium, pressure and velocity contours are aligned and slight meanders can be observed around the high orographies of the Rocky Mountains and the Tibetan Plateau. The velocity vectors are scaled linearly and the maximum velocities here reach 30 m/s.

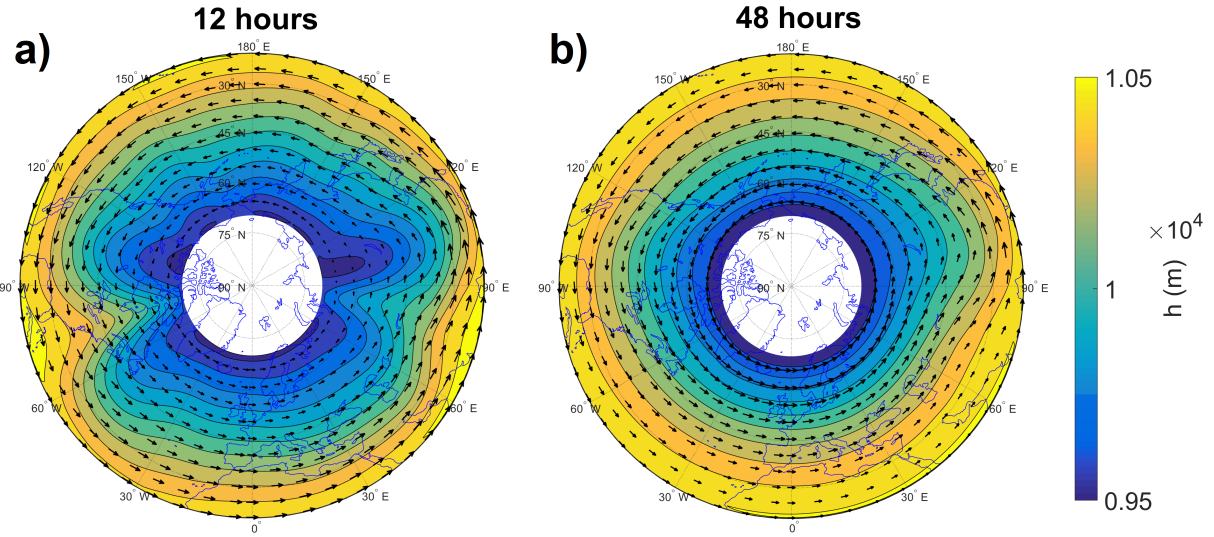


Figure 21: Lambert conformal conic projection of figure 20 with **a)** corresponding to 20b) and **b)** corresponding to 20c).

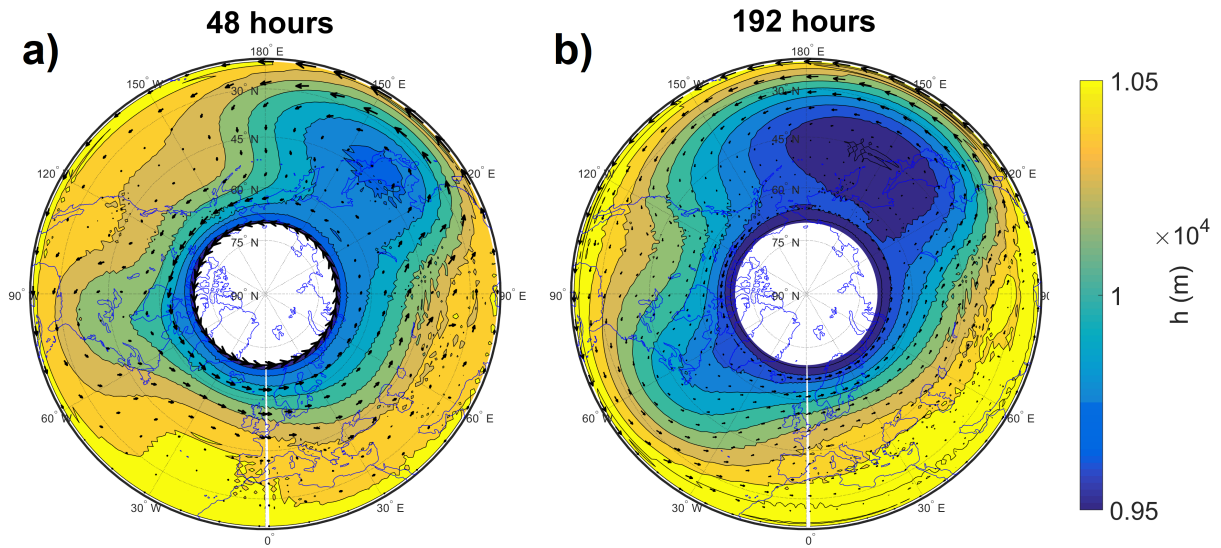


Figure 22: **a)** With the same initial- and boundary conditions conditions, much greater extent of meandering occurs in the model by Hogan, n.d where equations (12-14) are solved using a corrected Lax-Wendroff method (without curvature). **b)** Here, the highs and lows also evolve with time. That is, ζ is advected accordingly with (9). This is another feature that is not resolved in our own model likely due to the low order of accuracy of the Lax-Friedrich method. However, according to theory, large-scale Rossby waves propagate westward, against the zonal flow (Holton, 2004). This is not the case in Hogan's model. As can be observed, the highs and lows instead tend to propagate eastward with the flow while also expanding. Hence, there may be additional numerical- or model errors unaccounted for in ch. 2.2 and by Hogan. Note: Velocity scales in **a)** and **b)** are not the same.

5 Summary and Conclusions

Orographic Rossby waves are the main mechanism by which the jet streams meander around the Earth and have possibly far-reaching impacts on weather and climate (ch. 1). Hence, they are of particular importance to study and this project should serve as a starting point in what to consider when trying to model these waves. For example, we have to account for pressure gradients, Coriolis effect, orography, potential vorticity conservation and also Earth's curvature at this scale. These are covered in detail in ch. 2 and adapted to the Shallow Water Equations. In addition, some entry-level numerical techniques for solving these equations are presented throughout ch. 2.4 and then implemented for the global-scale Shallow Water Equations with conserved potential vorticity in ch. 3. The model is validated to work for typical shallow water flows in a bath tub and passes common tests like the Gaussian curve test (ch. 4.1). However, when considering atmospheric flows (ch. 4.2) it becomes evident that our model, as well as our numerical methods are lacking. Hence, a heavily modified version of Hogan's model is employed with a simplified numerical scheme. With these corrections, orographic Rossby waves appear to naturally form at appropriate locations. However, they do not fully exhibit the expected behaviours discussed in ch. 2.2. Even Hogan's model appears to have severe limitations as waves propagate in the wrong direction. Hence, this study is not complete and warrants further development in order to be useful.

6 Acknowledgements

I'd like to thank Drs. Björn Claremar and Erik Sahlée for taking their time to address questions I've had throughout the project. I'd also like to extend major thanks to Drs. Jon Shiach and Paul Ullrich for their excellent video courses on numerical methods for PDEs and atmospheric dynamics respectively. Although not explicitly related to this project, Prof. Nathan Kutz has given me great motivation in his video courses on numerical modelling and provided great instructions on how to implement spectral methods which I'm currently adapting the shallow water equations for. This should hopefully alleviate many of the issues encountered throughout this project.

References

- Blunden, J., D. S. Arndt, & M. O. Baringer (2011). State of the Climate in 2010. *Bulletin of the American Meteorological Society* 92.6, S1–S236.
- Hanna, E., T. E. Cropper, R. J. Hall, & J. Cappelen (2016). Greenland Blocking Index 1851–2015: a regional climate change signal. *International Journal of Climatology* 36.15, pp. 4847–4861.
- Payne, A. E. & G. Magnusdottir (2014). Dynamics of Landfalling Atmospheric Rivers over the North Pacific in 30 Years of MERRA Reanalysis. *Journal of Climate* 27.18, pp. 7133–7150.
- Baggett, C., S. Lee, & S. Feldstein (2016). An Investigation of the Presence of Atmospheric Rivers over the North Pacific during Planetary-Scale Wave Life Cycles and Their Role in Arctic Warming. *Journal of the Atmospheric Sciences* 73.11, pp. 4329–4347.
- Tedesco, M., T. Mote, X. Fettweis, E. Hanna, J. Jeraratnum, J. Booth, R. Datta, & K. Briggs (2016). Arctic cut-off high drives the poleward shift of a new Greenland melting record. *Nature Communications* 7.
- Stroeve, J. C., V. Kattsov, A. Barrett, M. Serreze, T. Pavlova, M. Holland, & W. N. Meier (2012). Trends in Arctic sea ice extent from CMIP5, CMIP3 and observations. *Geophysical Research Letters* 39.16. L16502.
- Warner, T. (2011). *Numerical weather and climate prediction*. Cambridge New York: Cambridge University Press.
- Hudson, J. (2001). *Numerical Techniques for Morphodynamic Modelling*. Reading, UK: University of Reading.
- Tan, W. (1992). *Shallow Water Hydrodynamics: Mathematical Theory and Numerical Solution for a Two-dimensional System of Shallow-water Equations*. Elsevier Oceanography Series. Elsevier Science, pp. 314–315.
- Holton, J. R. (2004). *An introduction to dynamic meteorology*. 4th ed. International Geophysics Series. Burlington, MA: Elsevier Academic Press, p. 535.
- Yazici, Y. (2010). *Operator Splitting Methods for Differential Equations*. Master thesis. Izmir: Izmir Institute of Technology.

Internet Resources

- Hogan, R. (n.d.). *Shallow Water Model in Matlab*. [Link](#). [2017-05-24].
- NOAA/NWS (n.d.). *The Jet Stream*. [Link](#). [2017-05-22].
- Tryggvason, G. (2011). *AME 90936 Computational Fluid Mechanics*. [Link](#). [2017-05-14].

7 Software

- Software name: MATLAB®
- Developer: The MathWorks, Inc.
- Year: 2016
- Version: R2016a
- Available at: <https://mathworks.com/>

© 2017 The MathWorks, Inc. MATLAB and Simulink are registered trademarks of The MathWorks, Inc. See mathworks.com/trademarks for a list of additional trademarks. Other product or brand names may be trademarks or registered trademarks of their respective holders.

Appendices

A Additional Numerical Methods

A.1 Dimensional Splitting

Dimensional splitting involves splitting up an N -dimensional PDE into a set of N 1-dimensional PDEs. Essentially, when applied to (16), which has the form $U_t + F(U)_x + G(U)_y = S$, then dimensional splitting allows us to rewrite this system as follows:

$$(16) \implies \begin{cases} U_t^* + F(U)_x = 0 \\ U_t + G(U^*)_y = S(U^*). \end{cases} \quad (19)$$

We solve this system by first approximating the first equation in a predictor step using a FDS, giving us the predictor solution U^* . We then use this as an initial condition for approximating the second equation, using the same FDS. This method however imposes a splitting error as well which normally has to be accounted for (Yazici, 2010).

A.2 Artificial Viscosity

Accordingly with Tryggvason, 2011, artificial viscosity for the Lax-Wendroff method ultimately takes the following form:

$$\begin{aligned} \text{Artificial Viscosity} &= \frac{1}{2} \left(\frac{\Delta t}{\Delta x} \right)^2 (U_{i+1,j}^n - 2U_{i,j}^n + U_{i-1,j}^n) \\ &\quad + D \frac{\Delta t}{\Delta x} \left[\left| U_{i+1,j}^n - U_{i,j}^n \right| (U_{i+1,j}^n - U_{i,j}^n) \right. \\ &\quad \left. - \left| U_{i,j}^n - U_{i-1,j}^n \right| (U_{i,j}^n - U_{i-1,j}^n) \right], \end{aligned}$$

where $D \in \mathcal{O}(1)$ is a constant viscosity coefficient. This is simply added to the solution to filter out waves of high wavenumber.

B MATLAB Code

This section covers the code that was first used in ch. 4.1, but the same overall structures applies to the code used in ch. 4.2. The heavily modified version of Hogan's model cannot be attached due to copyright. For details, see Hogan, n.d.

B.1 Spatial Domain and Parameters

```
9 %% Spatial array:  
10 % grid size:  
11 Nx = 180; % # of grid pts in x-dir  
12 Ny = 88; % -''- in y-dir  
13 % spatial step sizes:  
14 dy = 111*1e3; % 111 km / 1 deg latitude  
15 dx = dy; % for low latitudes  
16 % limits: % min-max distances in x,y  
17 xmin = 0;  
18 xmax = Nx*dx;  
19 ymin = 0;  
20 ymax = Ny*dy;  
21 % distance vectors:  
22 x = (xmin-dx : dx : xmax+dx)'; % distances in x for grid pts  
23 y = (ymin-dy : dy : ymax+dy)'; % -''- in y -''-  
24 [X,Y] = meshgrid(x,y); % sets up 2D grid with x and y-values (gives directionality)  
25 % indices for domain of interest without ghost nodes:  
26 i = 2:Nx+2; % x-indices  
27 j = 2:Ny+2; % y-indices  
  
29 %% Define parameters:  
30 % time:  
31 t = 0; % initial time (s)  
32 tmax = 3600*24*30; % simulation time (30 days)  
33 dt_output = 3600; % how often to store output data  
34 % constants:  
35 g = 9.8; % acceleration due to gravity (m/s^2)  
36 Omega = 7.2921*1e-5; % Earth rotation rate  
37 a = 6.371*10^6; % Earth radius  
38 D = 1; % viscosity coefficient  
39 cfl = 0.5; % Courant number
```

B.2 Orography Pre-processing

```
46 %% Orography:  
47 % Earth orography:  
48 load topo % loads world orography data  
49 B = topo(90:90+88,1:360); % elevation function describing the topography  
50 %B = [B(:,end/2:end),B(:,1:end/2)]; % shift map if needed  
51 % interpolate/extrapolate orography to fit grid:  
52 xtopo = linspace(0,Nx*dx,size(B,2));  
53 ytopo = linspace(0,Ny*dy,size(B,1));  
54 [Xtopo,Ytopo] = meshgrid(xtopo,ytopo);  
55 B = interp2(Xtopo,Ytopo,B,X,Y,'spline');  
56 % set ocean floors (negative elevations) to 0:  
57 B = (B > 0).*B;  
58 % smooth out orography:  
59 B = filter2('gaussian',B');  
60 B = filter2('gaussian',B')*1.5077e-06; % filter adjustment  
61 % enforce periodic BCs for topography:  
62 B(:,1) = B(:,end-2);
```

B.3 Coriolis Parameter

```

72 % latitude span:
73 phi = linspace(0,88,Ny+3) .* pi/180; % create latitude vector the length of Ny+3
74 % beta approximation:
75 phi0 = median(phi); % tangent latitudinal degree
76 beta = 2*Omega*cos(phi0)/a; % beta-plane slope
77 f0 = 2*Omega*sin(phi0); % f at phi0
78 f = f0 + beta.* (Y-mean(y)); % linear approximation of f

```

B.4 Initial Conditions

```

90 %% Initial conditions:
91 % initial vector of conserved variables:
92 U0 = zeros(Ny+3,Nx+3,3);
93 % where: h = H + eta (total depth = mean depth + displacement from mean)
94 % and: U(:,:,1) = h, U(:,:,2) = u, U(:,:,3) = v.
95
96 % mean depth (linear profile from 5700 to 5500 m):
97 total_height = repmat(linspace(5700,5500,Ny+3)',1,Nx+3);
98 H = total_height - B; % mean depth of fluid
99 U0(:,:,:,1) = H; % zero initial displacement (h = H, or eta = 0)

```

B.4.1 Geostrophic Balance

```

101 % geostrophic wind:
102 [dh_dx,dh_dy] = gradient(U0(:,:,:,1));
103 U0(:,:,:,:,2) = -g./f.*dh_dy/dx; % per unit grid dx
104 U0(:,:,:,:,3) = g./f.*dh_dx/dy; % per unit grid dy
105 zeta0 = 0;
106 q = (f + zeta0)./H;

```

Note that the gradient function calculates the gradient relative to the grid itself where, implicitly $\Delta x = 1$, and hence does not account for the actual distances we defined earlier where $\Delta x = 111$ km. Hence, we divide the velocities by the real Δx and Δy respectively to get the actual gradient.

B.5 While-Loop

```

125 U = U0;
126 n = 1;
127 while t < tmax
128   %% Adaptive time step:
129   maxu = max(abs(U(:,:,2)) + sqrt(g*U(:,:,1))); % max velocity in x
130   maxv = max(abs(U(:,:,3)) + sqrt(g*U(:,:,1))); % max velocity in y
131   dt = cfl*dx/max([maxu,maxv]); % max allowable time step

```

B.6 Lax-Wendroff Scheme

The Lax-Wendroff steps in 2D are replicated by the following code inside the while-loop:

```

134 while t < tmax
135 ...
136   %% Lax-Wendroff: (solves system for one time step using LW)
137   % enforce boundary conditions:
138   U = bc(U);
139   % compute fluxes at n:
140   [F,G] = flux(U);
141   [S] = source(U);
142   % compute half-steps at n+1/2 using Lax-Friedrich scheme:
143   U_iph(j,i,:) = 0.5*(U(j,i+1,:)+U(j,i,:)) - ...
144     (0.5*dt/dx)*(F(j,i+1,:)-F(j,i,:));
145   U_jph(j,i,:) = 0.5*(U(j+1,i,:)+U(j,i,:)) - ...

```

```

146      (0.5*dt/dy)*(G(j+1,i,:)-G(j,i,:));
147 % compute fluxes at n+1/2:
148 [F_iph,~] = flux(U_iph);
149 [~,G_jph] = flux(U_jph);
150 % compute full step at n+1 using Leapfrog scheme:
151 U(j,i,:) = U(j,i,:) + dt*S(j,i,:);
152 (dt/dx)*(F_iph(j,i,:)-F_iph(j,i-1,:));
153 (dt/dy)*(G_jph(j,i,:)-G_jph(j-1,i,:));
154 %% Artificial viscosity:
155 % - excluded from paper -
156 %% Update t:
157 t = t + dt;
158 ...
159 end

```

where $\text{flux}(U)$ and $\text{source}(U)$ are just separate functions that calculate $F(U)$, $G(U)$, and $S(U)$ respectively:

```

1 function [F,G] = flux(U)
2
3 global g B
4 eta = U(:,:,1) - B;
5 K = 0.5*(U(:,:,2).^2 + U(:,:,3).^2); % K = 0.5*(u^2 + v^2)
6 F(:,:,1) = U(:,:,1).*U(:,:,2); % hu
7 F(:,:,2) = K + g.*eta; % K + g*h
8 F(:,:,3) = 0; % 0
9 G(:,:,1) = U(:,:,1).*U(:,:,3); % hv
10 G(:,:,2) = 0; % 0
11 G(:,:,3) = F(:,:,2); % K + g*h
12 end

1 function S = source(U)
2 global q a tanphi
3 S = zeros(size(U));
4 S(:,:,1) = 0; % 0
5 S(:,:,2) = U(:,:,1).*q.*U(:,:,3) ...
6 + tanphi.*U(:,:,2).*U(:,:,3) / a; % hqv + uv*tan(phi)/a
7 S(:,:,3) = -U(:,:,1).*q.*U(:,:,2) ...
8 - tanphi.*U(:,:,2).^2 / a; % -hqu - u^2*tan(phi)/a
9 end

```

B.7 Boundary Conditions

```

1 function U = bc(U)
2 global U0
3 % transient BCs for h at west boundary:
4 U(:,end,1) = U(:,end-2,1);
5 % pinned BCs for h at south-north edges of domain (in order to keep up pressure gradient):
6 U(1,:,:1) = U0(1,:,:1);
7 U(end,:,:1) = U0(end,:,:1);
8 % transient BCs for u at west, south, and north boundaries:
9 U(:,end,2) = U(:,end-2,2);
10 U(1,:,:2) = U(3,:,:2);
11 U(end,:,:2) = U(end-2,:,:2);
12 % transient BCs for v at west boundary:
13 U(:,end,3) = U(:,end-2,3);
14 % periodic BCs at east-west boundaries for h,u,v:
15 U(:,1,:) = U(:,end,:);
16 % pinned BCs for v (0 meridional velocity at north-south boundaries):
17 U(1,:,:3) = 0;
18 U(end,:,:3) = 0;
19 end

```

B.8 Dimensionally Split Lax-Friedrich Scheme

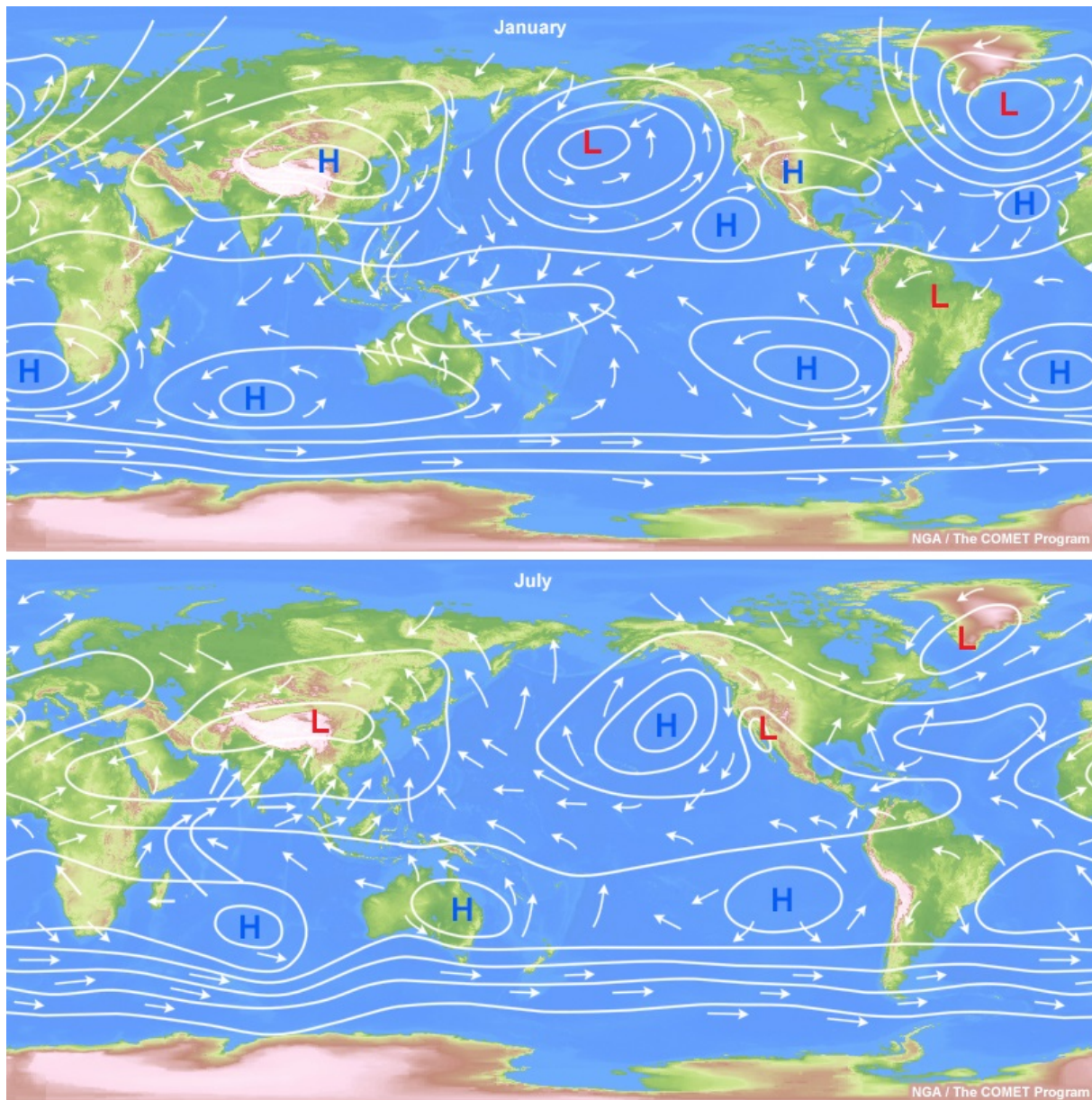
```

165 while t < tmax
166 ...
167 %% Lax-Friedrich:
168 % compute fluxes/sources/bcs:
169 U = bc(U);
170 [F,G] = flux(U);
171 S = source(U);
172 %% Lax-Friedrich (dimensionally split):
173 U(j,i,:) = 0.5*(U(j,i+1,:)+U(j,i-1,:)) ...
174     - 0.5*dt/dx*(F(j,i+1,:)-F(j,i-1,:));    % compute solution in x-direction (predictor
175 step)
176 U(j,i,:) = 0.5*(U(j+1,i,:)+U(j-1,i,:)) ...
177     - 0.5*dt/dy*(G(j+1,i,:)-G(j-1,i,:)) + dt*S(j,i,:);    % use predictor solution as
178 initial condition to compute solution in y-direction (corrector step)
179 ...
179 end

```

C Additional Figures

C.1 Semi-Permanent Pressure Zones



Geographical distribution of semi-permanent pressure zones in January (top) and July (bottom). Credit: NGA / The COMET Program. "The source of this material is the COMET® Website at <http://meted.ucar.edu/> of the University Corporation for Atmospheric Research (UCAR), sponsored in part through cooperative agreement(s) with the National Oceanic and Atmospheric Administration (NOAA), U.S. Department of Commerce (DOC). ©1997-2016 University Corporation for Atmospheric Research. All Rights Reserved."

